



ELSEVIER

Available online at www.sciencedirect.com

ScienceDirect

Proceedings of the Combustion Institute 000 (2022) 1–10

www.elsevier.com/locate/prociProceedings
of the
Combustion
Institute

Investigation of the effect of iron nanoparticles on n-dodecane combustion under external electrostatic fields

Efstratios Kritikos*, Andrea Giusti

Department of Mechanical Engineering, Imperial College London, South Kensington Campus, London SW7 2AZ, United Kingdom

Received 6 January 2022; accepted 1 July 2022

Available online xxx

Abstract

Reactive molecular dynamics simulations are performed to investigate the combined effects of iron nanoparticles and external electrostatic fields on the combustion of n-dodecane. Results suggest that iron nanoparticle additives significantly accelerate fuel and oxidizer consumption. In particular, the decomposition of n-dodecane is initiated at the nanoparticle's surface by hydrogen abstraction and subsequent absorption of the hydrogen and carbon atoms. Products, such as H_2 and H_2O , are formed in the nanoparticle's shell and released back into the gas phase, demonstrating a catalytic behaviour of the nanoparticle. Additionally, the application of an external electrostatic field further increases the n-dodecane consumption rate. A rise in the variety of product species is also observed when an external electrostatic field is applied due to the overall accelerated kinetics of the system. Analysis of the system's kinetic energy suggests that the presence of an external electrostatic field leads to an increase in the translational energy of the molecules. The chemical composition of the nanoparticle is also affected. The absorbed species diffuse along the surface of the nanoparticle to counteract the externally applied electric field. This species rearrangement leads to the formation of an anisotropic shell with varying chemical composition. This study suggests that the use of electrostatic fields with nanomaterial-based catalysis can offer new possibilities for the control of the reaction process as well as for the synthesis of tailored nanoparticles.

© 2022 The Author(s). Published by Elsevier Inc. on behalf of The Combustion Institute.

This is an open access article under the CC BY license (<http://creativecommons.org/licenses/by/4.0/>)*Keywords:* Nanoparticles; Electrostatic fields; Iron; n-Dodecane; Combustion; ReaxFF

1. Introduction

Metallic nanoparticles have recently gained significant attention in the combustion community, due to their high energy density and high surface-to-volume ratio compared to their micro-sized

* Corresponding author.

E-mail address: e.kritikos19@imperial.ac.uk (E. Kritikos).<https://doi.org/10.1016/j.proci.2022.07.003>1540-7489 © 2022 The Author(s). Published by Elsevier Inc. on behalf of The Combustion Institute. This is an open access article under the CC BY license (<http://creativecommons.org/licenses/by/4.0/>)

counterparts, resulting in high chemical reactivity, lower melting temperatures and increased catalytic activity [1]. The recent achievements in nanotechnology and synthesis of nanomaterials with tailored properties have further increased the interest in metal powder combustion [1], as well as in the use of nanoparticles to enhance the combustion properties of liquid fuels. The so-called *nanofuels*, i.e. suspensions of nanoparticles in a base liquid fuel, have been proposed as alternative fuels due to the possibility of increasing the energy density of the fuel and decreasing the emissions [2].

In particular, iron nanoparticles (FeNPs) combine many advantageous characteristics, which make them suitable to be used as energetic material and fuel additives. Iron is an easily available metal, which has low cost and is non-toxic [3]. Moreover, iron nano-powder is characterized by high burning rates [4]. In addition, the combustion temperature of FeNPs (around 2200 K) is comparable to that of hydrocarbon fuels [5]. Thus, FeNPs can preserve the solid-liquid state throughout the combustion process. Finally, the oxidation products consist of iron oxides, which can be filtered at the exhaust using particulate filtering technology and reduced back to pure iron by reacting with hydrogen [5]. Studies on the use of nanofuels with iron and aluminum oxide nanoparticles demonstrated an increase of heat release rates and thermal efficiency compared to the combustion of the base fuel [6].

Combustion of nanofuels is characterised by a wide range of scales and physical phenomena given by the interaction between nanomaterial, liquid fuel and gaseous phase [2]. Experiments on single droplet combustion have shown that the addition of nanoparticles could enhance the evaporation rate by offering sites for boiling nucleation. Shells of nanomaterial can form during the drying of the droplet and interact with the combustion of fuel vapour, or fragments of nanomaterial could be dispersed in the gas phase [2,7]. Sequential combustion of fuel vapour and metal nanoparticles has also been observed [8]. Studies on the oxidation process of nanoparticles at the molecular level [9–12] have shown that both diffusion and melt mechanisms are important elements of the combustion transient. Also, diffusion induced by electric charges has been identified as one of the mechanisms contributing to the oxidation of the nanoparticle [10]. Recent studies have focused on the mechanisms of adsorption of carbon-based fuels on the nanoparticle's surface [13], as well as on the effect of nanoparticles on hydrocarbon combustion [14]. It was shown that the presence of nanoparticles generally increases the reactivity of the system and the decomposition of the fuel through adsorption.

In addition to the development of alternative fuels, there is an increased attention towards electrification of the transportation and development of hybrid thermal-electric propulsion [15]. This means

that in next-generation engines there will be large availability of electrical energy that could be used to control the combustion process. External Electric Fields (EFs) have a direct effect on chemical reactions by affecting flame stabilization [16], blowoff limits [17] and flame shape [18], also showing in some cases a reduction of pollutant emissions [19]. Macroscale effects can be explained by the interactions at the atomistic level. On the one hand, external EFs determine the bulk movement of ionic species and electrons due to electrostatic forces and the movement of neutral species due to collisions with the charged species (ionic wind) [20]. On the other hand, the chemical evolution of the system is affected by the kinetics of polarized molecules, ions and electrons [21,22]. Reactive Molecular Dynamics (MD) studies showed that external EFs can influence directly the reaction rates, species consumption and initiation time of the combustion process [23,24].

In this work we study the combined effect of EFs and FeNPs on the combustion of hydrocarbons using reactive MD. n-Dodecane ($n\text{-C}_{12}\text{H}_{26}$) is used here as a surrogate for aviation fuels. The objectives are to: (i) investigate the role of FeNPs in the combustion kinetics of n-dodecane; (ii) analyse the effects of molecular polarization and local charge transfers on the consumption rates of fuel and oxidizer under external EFs; and (iii) study the mechanism of absorption of gas molecules into the FeNP and the related chemical composition of the nanoparticle with and without an external EF.

2. Methods

Reactive MD simulations are performed using the ReaxFF reactive force field [25], which can describe bond formation and dissociation during MD simulations. The high accuracy of ReaxFF arises from the fact that its parameters are tuned using quantum mechanics computations, while maintaining a relatively low computational cost even for large systems of atoms. In this study, the ReaxFF FeCHO-2016 [26] is used with a 0.3 bond order cut-off for the recognition of breaking and formation of bonds.

In the study of external EF effects on the reacting system, the computation of the charge distribution is of primary importance, since the Coulomb force is directly dependent to the atom's charge. In MD the charge distribution is computed by applying the Sanderson's Electronegativity Equalization (EE) principle [27] at each timestep. This method is based on the minimization of the system's electrostatic energy while satisfying the charge neutrality constraint. The Charge Equilibration (QEq) method [28] is the most widely used method to compute the atomic charges. However, the QEq method does not limit long-range charge transfers even between atoms of infinite separation, leading to spu-

rious net charges of neutral molecules [24,29,33]. This uncontrolled charge transfer, which could be a good approximation for conductive materials, involves the entire domain. Additionally, the QEq method lacks a description of polarization induced by an external EF.

To overcome these shortcomings the Charge Transfer with Polarization Current Equalization (QTPIE) method [33], which shields the charge transfers up to the overlap of the atomic orbitals and introduces molecular polarization under an external electric field, is used in this study. The overlap integrals are computed with the primitive Gaussian Type Orbitals (GTO). A short description of the derivation of the atomic exponential values for the GTO can be found in Section S1 of the Supporting Information. The QTPIE method is selected instead of other methods that perform a similar shielding of the charge transfers, such as the Split Charge Equilibration (SQE) [30] and the Atom-Condensed Kohn-Sham density functional theory to Second order approximation (ACKS2) [31], because it is formulated in the atom space instead of the bond space, thus reducing the computational cost [32]. Additionally, the QTPIE method has a similar formulation to the QEq method, thus the same ReaxFF can be used [24,33]. Finally, the QTPIE method includes a description of polarization due to an external EF that satisfies the non-locality constraint [34] and can be used with periodic boundary conditions in the direction of the EF [24]. It is worth noting that none of the aforementioned methods can describe ionization as there is no electron description in MD. Methods such as eReaxFF [35] include the particle nature of electrons and potentially can be further developed to be used in gas phase combustion simulations under external EFs (left for future study). Therefore, this study is limited to the investigation of electrostatic forces due to polarization and close charge transfers. It should also be noted that the conductivity of the metal nanoparticle under an external EF, where movement of charges towards the surface is expected (see Section 3.1), is sufficiently reproduced by the method used in this study.

An amorphous FeNP of 40 Å diameter, surrounded by 10 n-C₁₂H₂₆ and 185 O₂ molecules, was used in all simulations. The preparation procedure for the FeNP is detailed in Section S3. The FeNP is prepared to achieve a structure consistent with the nanoparticles reported in experimental studies (such as Ref. [36]). The preparation process of the nanoparticle is also important in order to eliminate any effects of the initial crystalline structure which has well-defined edges and faces and thus tends to have sharp melting points. The annealing process followed in this study is consistent with the one used in similar MD studies [11,37]. Molecules are placed in cubic boxes of densities 81.2 and 31.7 kg/m³ with periodic boundary conditions. The corresponding

gas mixture densities are 3.79 and 1.48 kg/m³, respectively. Fairly low densities are examined in this study compared to previous investigations, such as Ref. [11], in order not to significantly accelerate the oxidation process and fail to observe any effects of EFs. Both density systems are simulated at 1800 K. Additionally, temperature effects are studied for the 31.7 kg/m³ system with simulations at 1800 and 2000 K. Results are obtained for 5 external EFs, corresponding to $\mathcal{E} = 0$ (base case), 10^{-4} , 10^{-3} , 10^{-2} and 0.1 V/Å.

Simulations for all temperature, density and EF conditions are performed using both the micro-canonical (NVE) and canonical (NVT) ensembles. For the NVT ensemble, the Nosé-Hoover thermostat is used to regulate the temperature with a damping constant of 100 fs. Practically, the NVT simulations resemble the conditions of a combustor where a constant temperature is maintained. On the contrary, the process of NVE ensemble allows the investigation of the ignition and combustion transient of the system.

All simulations are performed using the LAMMPS software [38] equipped with the USER-REAXC package [39]. The cut-off distance for ghost atoms is modified to match the maximum overlap integral distance (see Section S1). The equations of motion are progressed using the Verlet algorithm with a timestep of 0.1 fs. The timestep is held sufficiently small to capture all reaction events at high temperatures [40]. For post-processing, the atomic connectivities and trajectories are outputted every 20 fs and 0.5 ps, respectively. Reactions are monitored for a total simulated time of 2 ns for NVT simulations and 1.5 ns for NVE simulations. Results for all studied conditions are averaged over 3 simulations, each initialised with the same atom positions and different velocities (sampled from a Maxwell-Boltzmann distribution) before the equilibration step.

The Kinetic Energy (KE) components, i.e. translational, rotational and vibrational, are computed based on the velocity of the molecule's center-of-mass, on its rotational movement and on the residual atomic motion, respectively. In addition, the shell thickness of the FeNP is measured as the distance of an absorbed C, H or O atom from the FeNP's surface. The FeNP's surface is computed based on the alpha-shape method [41] using a 4 Å radius and a smoothing level of 8. Additionally, the shell characteristics are evaluated separately on the front (i.e., the side with outward normal vector in the direction of the external EF) and back hemisphere of the FeNP. The front and back hemispheres are separated with a plane, normal to the direction of the EF and passing from the center-of-mass of the FeNP. This approach was selected to examine the shell thickness instead of the radial distribution function as under an external EF the FeNP loses its spherical shape.

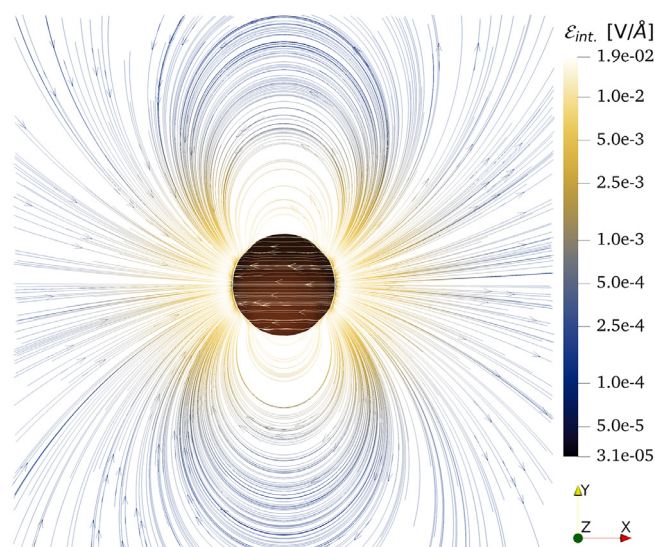


Fig. 1. Internal EF of a BCC FeNP with a lattice parameter $a = 2.866 \text{ \AA}$ under $\mathcal{E} = 0.1 \text{ V/\AA}$ along the x-direction; the internal EF is computed using a Fe sample charge placed in a 200-cell cubic grid; the Coulomb interactions were shielded using the γ parameter (as used in ReaxFF [25]) to account for close interactions between the sample charge and FeNP atoms.

3. Results and discussion

3.1. Polarization and charge distribution

The effect of the external EF on an isolated FeNP is first investigated. Theoretically, the external EF polarizes the conductive sphere, as the negatively charged electron cloud is pushed opposite to the EF direction, i.e. towards the back hemisphere of the FeNP. This charge rearrangement leads to an equal in magnitude and opposite internal EF, in order to cancel the external EF inside the nanoparticle. Polarization of the FeNP is succeeded with the QTPIE method as shown in Fig. 1 for an external EF along the x-direction with a strength of 0.1 V/\AA . The field lines follow the expected direction, i.e. they appear to be perpendicular to the surface and parallel inside the FeNP [42]. All charge is accumulated on the surface while the core's charge is equal to zero (see Fig. S1). The dipole moment of the FeNP predicted with the QTPIE method (e.g., $\mu_{\text{MD},10^{-2}\text{V/\AA}} = 3.8 \text{ D}$) is approximately 2 times lower than the theoretical value for a linearly polarized spherical conductor (e.g., $\mu_{\text{th},10^{-2}\text{V/\AA}} = 8.9 \text{ D}$) for all investigated EFs. This can be attributed to the shielding nature of the QTPIE method, which introduces a dielectric constant for the FeNP. Moreover, a weak polarization takes place between the surface atoms and the adjacent atoms (as is evident in Fig. S1). This is a consequence of the charge equilibration method, which is based on atomic positions without an explicit treatment of the electron cloud.

It should be noted that when the FeNP is immersed in a gas domain the nanoparticle acquires a small net charge, mainly caused by the charge equilibration that is performed on the entire system and not on individual molecules. In the case with low density we observe a net charge of -0.768 e for the whole FeNP. This net charge fluctuates during the simulation, due to close interactions with the gas molecules. Although relatively small, at very high EFs this net charge can cause a movement of the FeNP in the direction opposite to the direction of the external EF. For example, in NVT simulations at 31.7 kg/m^3 and 1800 K , the FeNP reaches a relatively constant velocity (after an initial acceleration) equal to 8 m/s and 38 m/s for EF strengths of 10^{-2} V/\AA and 0.1 V/\AA , respectively. This velocity is small compared to the average thermal velocity of the gas phase (e.g., $c_{\text{ave},\text{O}_2} = 1600 \text{ m/s}$) and should not considerably affect the results. Note that when the QEq charge equilibration method is applied, the net charge of the FeNP becomes about 51.1 e (see Fig. S2). This demonstrates some success of the method adopted here in achieving charge shielding and limiting long-range charge transfers.

3.2. Kinetics

The FeNP acts as a catalyst when inserted into the gas mixture. Under the same ambient conditions, gas-only simulations predicted no reactions during the first 4 ns of simulation (not shown here). To evaluate the accuracy of these simulations the activation energies of selected combustion reactions were evaluated with the ReaxFF

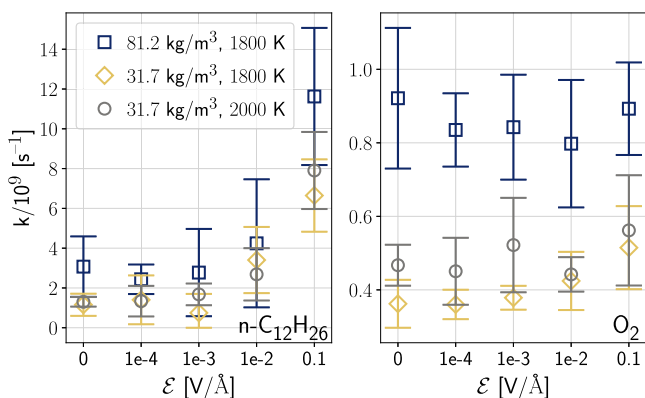


Fig. 2. First-order rate constants of $n\text{-C}_{12}\text{H}_{26}$ and O_2 consumption derived from NVT ensemble simulations.

FeCHO-2016. Good agreement with the literature was found (as shown in Section S5). It should be noted that combustion of $n\text{-C}_{12}\text{H}_{26}$ is initiated through pyrolysis at high temperatures [43]. A detailed analysis of n -dodecane combustion under external electrostatic fields can be found in Ref. [44]. On the contrary, when FeNPs are included in the domain, dissociation and oxidation reactions take place in the first 10 ps of the simulated time. Figs. 2 and 3 show the rate constants (from NVT simulations) and time evolution of species, respectively. Under no external EF an increase in temperature or density accelerates the consumption of both $n\text{-C}_{12}\text{H}_{26}$ and O_2 . Both fuel and oxidizer molecules react with the FeNP's surface, dissociate and get absorbed, resulting in highly accelerated kinetics compared to the gas-only simulations. As the fuel and oxidizer dissociate an increase in the formation of H_2 and H_2O gas products is noted, even at the initial stages of combustion. These products are formed on the surface of the FeNP and escape into the gas mixture. No carbon products are observed in the gas phase since C atoms remain absorbed into the FeNP. Towards the final stage of the simulated time the FeNP is melting, leading to the release of a few iron compounds as recorded in some cases of both NVT and NVE ensemble simulations.

Regarding the influence of the external EF on the kinetics of the system, for $\mathcal{E} \leq 10^{-3} \text{ V/\AA}$ no significant effects are observed, as any changes of the average consumption rate lie within the statistical uncertainties (Fig. 2). Similarly, no considerable change in the time evolution of products is noted. On the contrary, for $\mathcal{E} \geq 10^{-2} \text{ V/\AA}$ a clear effect on the consumption rate of $n\text{-C}_{12}\text{H}_{26}$ is observed for all studied conditions (both NVT and NVE simulations). The consumption of O_2 seems unaffected in NVT simulations, except for the case at 31.7 kg/m^3 and 1800 K , where a slight increase of the average first-order rate constant is observed for

$\mathcal{E} \geq 10^{-2} \text{ V/\AA}$. In NVE simulations a clear acceleration of O_2 consumption takes place for all studied conditions when $\mathcal{E} = 0.1 \text{ V/\AA}$ (not shown here). In gas-only simulations, no reactions occurred in a 4 ns simulated time even under strong external EFs. Therefore, simulations suggest that EFs are more effective when combined with FeNPs, enhancing the catalytic action of the nanomaterial. It should be noted that, due to the small amount of charge transfer, only relatively high EFs show effects on the system dynamics in the timeframe investigated here. At such strong EFs, ionization may be expected, which requires further investigation and the development of new methods that take into account free electrons and ionic species.

In addition, under the strong 0.1 V/\AA EF, production of simpler hydrocarbons is noted. Observing the trajectories of $n\text{-C}_{12}\text{H}_{26}$, it is evident that these molecules originate from fuel pyrolysis. The kinetics is affected by the close interactions and the related charge transfers between the FeNP and gas molecules, which results in a translational acceleration when an external EF is applied. In general, the strong EF leads to a reduction in the total number of C, H and O compound molecules, such as H_2O , in the gas phase. Additionally, the production of other oxygen compound species, such as OH and CO, is evident mostly for the strong EF. In NVE ensemble simulations at $\mathcal{E} = 0.1 \text{ V/\AA}$, the FeNP quickly melts forming many smaller iron clusters which subsequently further catalyse the gas phase mixture. Therefore, the strong EF leads to a large variety of different species but to an overall smaller number of molecules in the gas phase.

To further investigate the kinetics of the system, the KE components of the last nanosecond of the total simulated time are analysed in Fig. 4. In absence of an external EF, the FeNP has high vibrational energy while its translational energy is negligible due to the system's homogeneity. Conversely, the gas molecules experience primarily translational

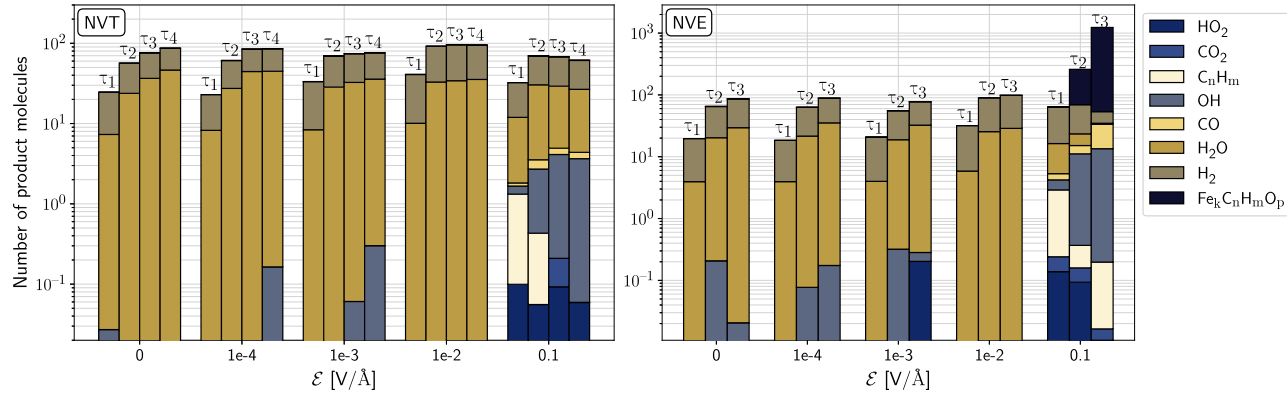


Fig. 3. Number of molecules of products for the NVT (left) and NVE (right) simulations for 31.7 kg/m^3 and 1800 K condition, averaged over consecutive time periods of 500 ps (i.e., $\tau_1 = \tau_2 = \tau_3 = \tau_4 = 500 \text{ ps}$); note the logarithmic scale of the y-axis. The numerical values are also reported in Table S4.

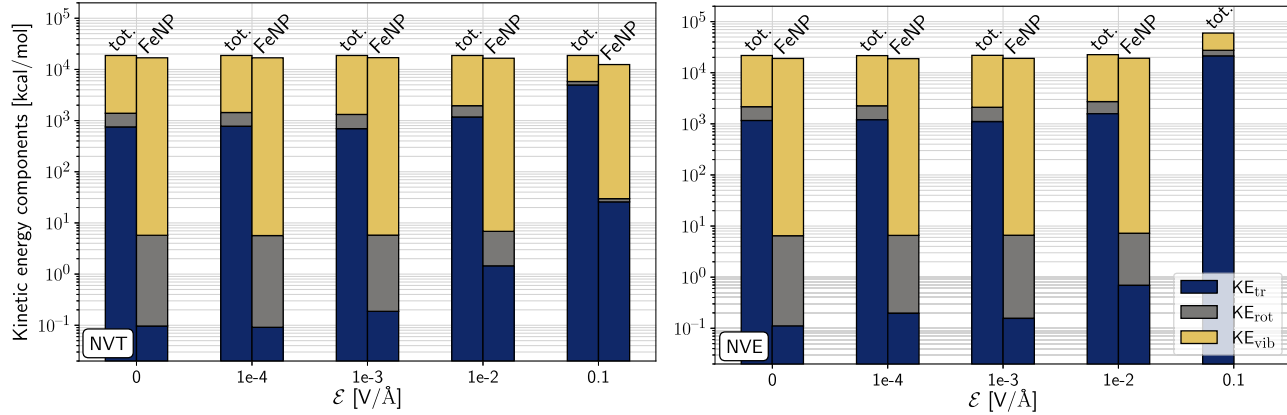


Fig. 4. KE components from NVT (left) and NVE (right) simulations for 31.7 kg/m^3 and 1800 K condition, averaged over the last nanosecond of the total simulated time. The numerical values are also reported in Table S5.

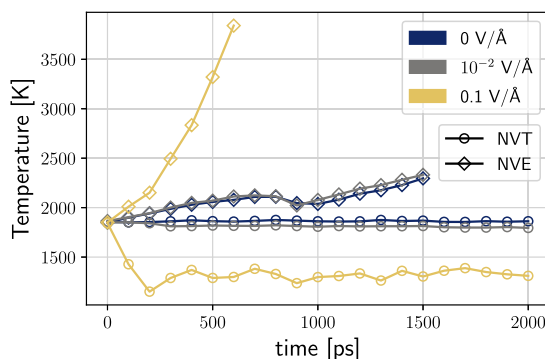


Fig. 5. Temperature of FeNP for 31.7 kg/m^3 and 1800 K condition.

movement. For example, in NVT simulations at 31.7 kg/m^3 and 1800 K, the translational, rotational, and vibrational KEs of the gas mixture are 752, 634 and 462 kcal/mol respectively. The low vibrational energy of the gas mixture can be attributed to the fact that only a few to no $n\text{-C}_{12}\text{H}_{26}$ molecules (typically characterised by high vibrational energy) exist, whilst O_2 experiences primarily rotational movement. For weak EFs there are negligible fluctuations of the KE components, which verifies that the effects of the external EF on the system's kinetics are not significant. For strong EFs ($\mathcal{E} \geq 10^{-2} \text{ V/\AA}$) an increase in translational KE of both the system and the FeNP is observed. The FeNP's movement is mainly affected by the small but non-negligible net negative charge that the FeNP acquires when placed inside the domain with the gas mixture. As discussed in Section 3.1, this residual charge can be primarily attributed to the formulation of the QTPIE method. Nonetheless, the translation KE of the gas is increased mainly due to the non-negligible net charge that the fuel and oxidizer molecules can acquire as they closely interact. A decrease in the vibrational KE, both for the FeNP and system, can be observed, suggesting stabilization effects of the external Coulomb force. Effects are not as evident in NVE ensemble simulations at $\mathcal{E} = 10^{-2} \text{ V/\AA}$ due to the accelerated kinetics of the system which overcomes the effect of electrostatic forces. It is noted that the FeNP's KEs are not reported for $\mathcal{E} = 0.1 \text{ V/\AA}$ in NVE ensemble simulations as the FeNP starts to melt and fragment after the first 0.6 ns of simulated time.

Fig. 5 shows the FeNP temperature as a function of time, computed from the atomic kinetic energies under different external EFs and ensembles (the temperature of the system is shown in Fig. S4). Results only for the base case and high-strength EFs are shown, since, as previously explained, no significant difference was observed for weaker strengths of the external EF. Differences between the NVT and NVE ensemble simulations can be observed. In NVT simulations there is a decrease

in the FeNP temperature, i.e. KE, especially under very strong external EF. Any temperature changes take place in the first 500 ps of the simulated time. Afterwards, the temperature remains constant. The decrease of nanoparticle temperature is mainly due to the effects of the thermostating method and the presence of drift velocities under the external Coulomb force. This suggests that the development of new thermostating strategies in the presence of external variable forces should be addressed in future research [45,46]. On the contrary, in NVE simulations an increase in the atomic velocities and consequently in the FeNP's and system's temperature is observed. A local minimum is noted around 1 ns of simulated time for $\mathcal{E} \leq 10^{-2} \text{ V/\AA}$, which corresponds to the FeNP's melt. Specifically, this decrease in KE is attributed to the transition from solid to liquid phase since at 0.9 ns time the BCC structure of the FeNP is completely lost. Results for $\mathcal{E} = 0.1 \text{ V/\AA}$ are presented until the melt and decomposition of the FeNP.

3.3. Chemical reactions

The combustion mechanism of gas mixture and FeNP begins with absorption and dissociation of hydrocarbon and oxygen molecules, which is an exothermic process [11,47]. The initiation time of absorption, which denotes the time till the first reaction between a gas molecule and the FeNP occurs, suggests that O_2 is the first species to get absorbed at 1800 K (see Table S3). The chemical absorption mechanism of $n\text{-C}_{12}\text{H}_{26}$ in the FeNP is presented in Fig. S5. Firstly, bonds between Fe atoms and the H atoms are formed. Secondly, the C-H bonds break and the H atoms get absorbed at the surface. Subsequently, the bonds between the C and Fe atoms are formed, which suggests that the carbon chain gets absorbed at the surface. Finally, the C-C bonds break as well. It is evident that $n\text{-C}_{12}\text{H}_{26}$ molecules undergo dehydrogenation instead of pyrolysis. This result is in agreement with the study of Zhang et al. [13] for the reaction of

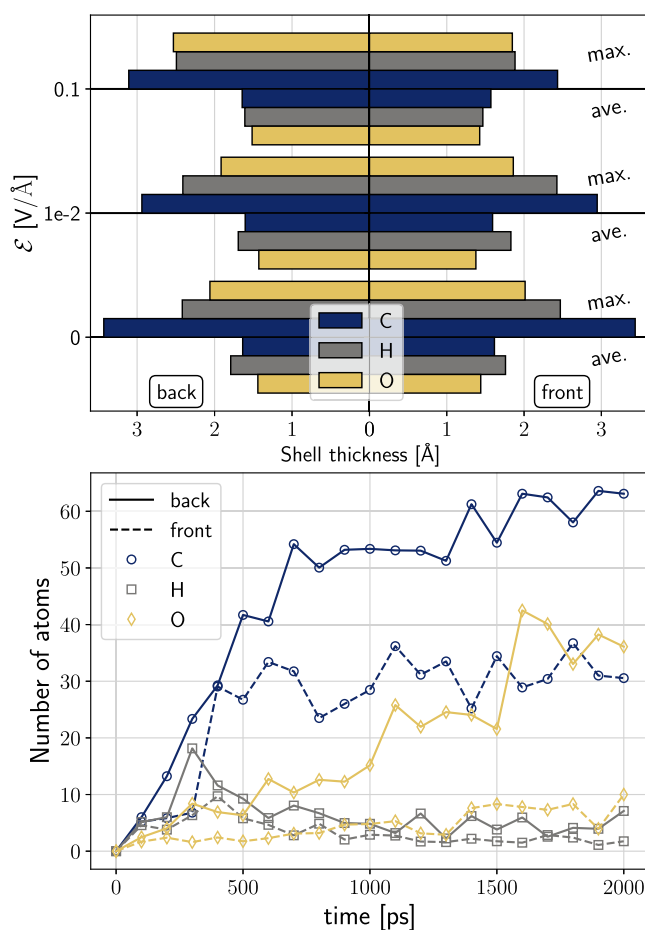


Fig. 6. Shell thickness for each species (top) and number of absorbed atoms in the FeNP at 0.1 V/\AA (bottom); results are presented for NVT simulations for 31.7 kg/m^3 and 1800 K .

ethanol over aluminum nanoparticles. This results in a very rapid dissociation of $n\text{-C}_{12}\text{H}_{26}$, which leads to a significant heat release. It is noted that the number of C–C bonds remains constant at 6 since many C_2 structures exist on the surface of the nanoparticle. Also the number of Fe–C bonds remains constant, which suggests that no carbon compounds escape back to the gas phase. Moreover, the number of Fe–H bonds decreases due to the fact that hydrogen compound species are emitted into the gas phase. A similar absorption mechanism is observed both in simulations without an external EF and when a 0.1 V/\AA EF is applied (see Fig. S5).

The next stage of the FeNP combustion corresponds to core melt and to diffusion of core atoms towards the surface of the nanoparticle [12]. This effect is more evident in the NVE ensemble simulations where the temperature is governed by the reactions, thus the temperature increases significantly. In NVT ensemble simulations the temper-

ature effect on FeNP is in the form of local hot-spots and high-temperature areas [11]. The combustion of the nanoparticle continues further with an inward diffusion of shell atoms and outward diffusion of core atoms [12]. This diffusion is driven by an induced EF between the positively charged core and the negatively charged shell, as also reported in previous studies [9,10]. For example, at 2 ns of an NVT simulation at 31.7 kg/m^3 , 1800 K and zero EF the FeNP has a net charge of -0.84 e . The core (defined here as a sphere of 12 \AA radius from the center-of-mass) has a charge of 0.18 e , while the shell has a charge of -1.03 e . It is evident that the non-bonded van der Waals and Coulomb interactions have a significant effect on the combustion process of nanoparticles. It is interesting that this phenomenon of core atom diffusion towards the surface and inward diffusion of shell atoms takes place even with the QTPIE method that predicts lower charges than the QEq method, which other studies used. As previously discussed,

products, such as H_2 and H_2O , are formed into the nanoparticle and released to the gas phase. As a result, the FeNP seems to accelerate the combustion process by quickly catalysing the fuel and oxidizer into smaller products.

The external EF can alter the local thickness and composition of the FeNP's shell. After gas molecules dissociate and get absorbed into the nanoparticle, they acquire a negative charge and thus diffuse along the surface towards the back hemisphere of the FeNP, due to the Coulombic force, in order to counteract the external EF. For example, at 2 ns of an NVT simulation at 31.7 kg/m^3 , 1800 K and 0.1 V/\AA EF the FeNP has a net charge of $-0.44 e$. The front and back hemispheres of the core have a charge equal to $0.06 e$ and $0.38 e$, respectively, while the front and back sides of the shell have a charge of $0.46 e$ and $-1.34 e$. This diffusion leads to an anisotropic FeNP shell structure. Fig. 6 shows the shell thickness of the front and back hemispheres of the FeNP from the NVT ensemble simulations. Under no external EF there is a uniform thickness between the front and back sides. Similarly, for $\mathcal{E} < 10^{-2} \text{ V/\AA}$ no significant difference on the local shell thickness appears. However, for $\mathcal{E} = 10^{-2} \text{ V/\AA}$ there is a decrease in the overall maximum and average shell thicknesses. This can be attributed to the fact that after the movement of negatively charged C, H and O atoms to the back side of the FeNP, the Coulomb force opposes the inward diffusion towards the core. Similar considerations can be applied for the strong EF. Specifically, even if there are many more atoms on the back side (as shown in Fig. 6), the Coulomb force keeps them near the surface. Note that the average shell thickness, which indicates the distance of absorbed C, H, and O species from the surface of the FeNP, does not show significant differences between the front and back side of the FeNP (for all EFs).

From Fig. 6 it can also be observed that the number of atoms in the back side of the FeNP is significantly higher than that in the front side for all species. We note that the number of C and O atoms absorbed into the FeNP keeps increasing with time. However, the number of H atoms initially increases and then decreases with time. This can be attributed to the fact that H_2 and H_2O molecules are formed and escape from the FeNP's surface. Hence, less H atoms can be found absorbed into the FeNP. Additionally, only a small percentage of absorbed O atoms can be found in the front hemisphere. The faster diffusion of O atoms towards the back side occurs due to the higher negative charge they can acquire. Finally, the existence of more species on the back side of the FeNP leads to partial melting of the back area, which can result in detachment and release of Fe compounds into the gas phase. The shell thickness of the FeNP obtained from the NVE simulations is shown in Fig. S6. Sim-

ilarly to the NVT simulations, a uniform shell composition is observed when no EF is applied. Under a 0.1 V/\AA EF the reactivity of the system drastically increases, which leads to the rapid formation of a thick shell. This increase in reactivity is associated with the quick increase of the FeNP's temperature, as shown in Fig. 5. It is noted that, similarly to the NVT simulations, the external EF leads to an anisotropic chemical composition of the FeNP. As shown in Fig. S6, the front and back sides of the FeNP have a different number of absorbed C, H and O atoms.

4. Conclusions

A reactive molecular dynamics study of the interaction of iron nanoparticles with $n\text{-C}_{12}\text{H}_{26}$ combustion has been performed, with a focus on the effect of externally applied electrostatic fields. The presence of an iron nanoparticle increases the reactivity of the system, which is further accelerated by the external electrostatic field. The increase in reactivity is related to the rapid dissociation and absorption of fuel and oxidizer into the nanoparticle. It was found that $n\text{-C}_{12}\text{H}_{26}$ undergoes dehydrogenation induced by the nanoparticle, instead of following a pyrolysis reaction path typically found at high temperature without nanoadditives. Under strong external electrostatic fields, a further acceleration of the fuel's consumption is observed. On the contrary, in most cases the external electric field does not significantly affect the consumption rate of O_2 . Additionally, for strong electric fields a larger variety of gas-phase species was recorded as an indication of enhanced catalytic effects. The diffusion of atoms into the nanoparticle is also affected by the external electric field. As the fuel and oxidizer dissociate and get absorbed, the respective atoms acquire a negative charge and diffuse towards one side of the nanoparticle to balance the external electric field. As a result, the electric field leads to an anisotropic shell thickness and chemical composition.

This study opens up new possibilities for the control of the combustion process through the combination of tailored nanofuels and electrostatic fields. This study also suggests that electrostatic fields could potentially be used for the synthesis of nanoparticles with varying properties across the surface.

Declaration of Competing Interest

The authors declare that they have no known competing financial interests or personal relationships that could have appeared to influence the work reported in this paper.

Supplementary material

Supplementary material associated with this article can be found, in the online version, at doi:10.1016/j.proci.2022.07.003.

References

- [1] R.A. Yetter, G.A. Risha, S.F. Son, *Proc. Combust. Inst.* 32 (2) (2009) 1819–1838.
- [2] S. Basu, A. Miglani, *Int. J. Heat Mass Transf.* 96 (2016) 482–503.
- [3] J.M. Bergthorson, *Prog. Energy Combust. Sci.* 68 (2018) 169–196.
- [4] J.A. Styborski, M.J. Scorza, M.N. Smith, M.A. Oehlschlaeger, *Propellants Explos. Pyrotech.* 40 (2) (2015) 253–259.
- [5] J.M. Bergthorson, S. Goroshin, M.J. Soo, P. Julien, J. Palecka, D.L. Frost, D.J. Jarvis, *Appl. Energy* 160 (2015) 368–382.
- [6] M. Nouri, A.H.M. Isfahani, A. Shirneshan, *Clean Technol. Environ. Policy* (2021).
- [7] I. Javed, S.W. Baek, K. Waheed, *Combust. Flame* 162 (1) (2015) 191–206, doi:10.1016/j.combustflame.2014.07.015.
- [8] Y. Gan, L. Qiao, *Combust. Flame* 158 (2) (2011) 354–368.
- [9] B.J. Henz, T. Hawa, M.R. Zachariah, *J. Appl. Phys.* 107 (2) (2010) 024901.
- [10] P. Chakraborty, M.R. Zachariah, *Combust. Flame* 161 (5) (2014) 1408–1416.
- [11] S. Hong, A.C. Van Duin, *J. Phys. Chem. C* 119 (31) (2015) 17876–17886.
- [12] G. Li, L. Niu, W. Hao, Y. Liu, C. Zhang, *Combust. Flame* 214 (2020) 238–250.
- [13] Y.R. Zhang, A.C.T. van Duin, K.H. Luo, *Fuel* 234 (2018) 94–100.
- [14] M. Lucas, S.J. Brotton, A. Min, C. Woodruff, M.L. Pantoya, R.I. Kaiser, *J. Phys. Chem. A* 124 (8) (2020) 1489–1507, doi:10.1021/acs.jpca.9b10697.
- [15] B.J. Brelje, J.R.R.A. Martins, *Prog. Aerosp. Sci.* 104 (2019) 1–19.
- [16] M.K. Kim, S.H. Chung, H.H. Kim, *Combust. Flame* (2012).
- [17] M.K. Kim, S.K. Ryu, S.H. Won, S.H. Chung, *Combust. Flame* 157 (1) (2010) 17–24.
- [18] Y. Ren, W. Cui, S. Li, *Phys. Rev. E* 97 (1) (2018) 013103.
- [19] E.V. Vega, S.S. Shin, K.Y. Lee, *Fuel* 86 (4) (2007) 512–519.
- [20] J. Lawton, *Electrical aspects of combustion*, 1969.
- [21] S. Shaik, D. Mandal, R. Ramanan, *Nat. Chem.* 8 (12) (2016) 1091–1098.
- [22] B.N. Ganguly, *Plasma Phys. Controlled Fusion* 49 (12B) (2007) B239–B246.
- [23] S. Tan, T. Xia, Y. Shi, J. Pfaendtner, S. Zhao, Y. He, *Sci. Rep.* 7 (1) (2017) 1–11.
- [24] E. Kritikos, A. Giusti, *J. Phys. Chem. A* 124 (2020). acs.jpca.0c08040
- [25] A.C.T. Van Duin, S. Dasgupta, F. Lorant, W.A. Goddard III, *J. Phys. Chem. A* 105 (41) (2001) 9396–9409.
- [26] M.M. Islam, C. Zou, A.C.T. Van Duin, S. Raman, *PCCP* 18 (2) (2015) 761–771.
- [27] R.T. Sanderson, *Science* 114 (2973) (1951) 670–672.
- [28] A.K. Rappé, W.A. Goddard, *J. Phys. Chem.* 95 (8) (1991) 3358–3363.
- [29] J.P. Koski, S.G. Moore, R.C. Clay, K.A. O’Hearn, H.M. Aktulga, M.A. Wilson, J.A. Rackers, J.M.D. Lane, N.A. Modine, *J. Chem. Theory Comput.* (2021), doi:10.1021/acs.jctc.1c00975. acs.jctc.1c00975
- [30] D. Mathieu, *J. Chem. Phys.* 127 (22) (2007) 224103.
- [31] T. Verstraelen, P.W. Ayers, V. Van Speybroeck, M. Waroquier, *J. Chem. Phys.* 138 (7) (2013).
- [32] J. Chen, D. Hundertmark, T.J. Martinez, *J. Chem. Phys.* 129 (21) (2008).
- [33] J. Chen, T.J. Martinez, *Chem. Phys. Lett.* 438 (4–6) (2007) 315–320.
- [34] J. Chen, *Theory and applications of fluctuating-charge models*, University of Illinois at Urbana-Champaign, 2009 Ph.D. thesis.
- [35] M.M. Islam, G. Kolesov, T. Verstraelen, E. Kaxiras, A.C. Van Duin, *J. Chem. Theory Comput.* 12 (8) (2016) 3463–3472.
- [36] D.L. Huber, *Small* 1 (5) (2005) 482–501.
- [37] J. Sun, S. Hui, P. Liu, R. Sun, M. Wang, *Coatings* 9 (6) (2019).
- [38] S. Plimpton, *J. Comput. Phys.* (1995).
- [39] H.M. Aktulga, J.C. Fogarty, S.A. Pandit, A.Y. Grama, *Parallel Comput.* 38 (4–5) (2012) 245–259.
- [40] K. Chenoweth, A.C.T. van Duin, W.A. Goddard, *J. Phys. Chem. A* 112 (5) (2008) 1040–1053.
- [41] A. Stukowski, *JOM* 66 (3) (2014) 399–407.
- [42] D.J. Griffiths, *Introduction to Electrodynamics*, Pearson Education, Inc., 2013.
- [43] K.M. Bal, E.C. Neyts, *Chem. Sci.* 7 (8) (2016) 5280–5286.
- [44] E. Kritikos, A. Lele, A.C. van Duin, A. Giusti, *Combust. Flame* (2022).
- [45] Y. Zhao, G. Morales, *Phys. Rev. E* 98 (2) (2018) 022213.
- [46] G. Morales, *Phys. Rev. E* 99 (6) (2019) 062218.
- [47] X. Chang, Q. Chu, D. Chen, *J. Phys. Chem. C* 124 (24) (2020) 13206–13214.